

A View-consistent Sampling Method for Regularized Training of Neural Radiance Fields

Aoxiang Fan¹, Corentin Dumery¹, Nicolas Talabot¹, Pascal Fua¹

¹Computer Vision Laboratory, EPFL, Switzerland

{aoxiang.fan, corentin.dumery, nicolas.talabot, pascal.fua}@epfl.ch

Abstract

Neural Radiance Fields (NeRF) has emerged as a compelling framework for scene representation and 3D recovery. To improve its performance on real-world data, depth regularizations have proven to be the most effective ones. However, depth estimation models not only require expensive 3D supervision in training, but also suffer from generalization issues. As a result, the depth estimations can be erroneous in practice, especially for outdoor unbounded scenes. In this paper, we propose to employ view-consistent distributions instead of fixed depth value estimations to regularize NeRF training. Specifically, the distribution is computed by utilizing both low-level color features and high-level distilled features from foundation models at the projected 2D pixel-locations from per-ray sampled 3D points. By sampling from the view-consistency distributions, an implicit regularization is imposed on the training of NeRF. We also utilize a depth-pushing loss that works in conjunction with the sampling technique to jointly provide effective regularizations for eliminating the failure modes. Extensive experiments conducted on various scenes from public datasets demonstrate that our proposed method can generate significantly better novel view synthesis results than state-of-the-art NeRF variants as well as different depth regularization methods.

1. Introduction

3D scene reconstruction from multiple images is a long-standing vision problem [11] but the recent advent of Neural Radiance Fields (NeRFs) [28] has delivered a significant performance boost, especially given a dense set of input images. However, in much the same way the old shape-from-shading was ill-posed [32], so is the NeRF reconstruction problem: as shown in [62], in the absence of explicit or implicit regularization, a set of training images can be fitted independently of the recovered geometry. This phenomenon,

known as shape-radiance ambiguity, is particularly evident when the input views are not dense enough, even though using Multi-Layer Perceptrons (MLPs) for scene representation weakly regularizes the scene reconstructions [60, 62].

Many kinds of regularizers have been proposed to improve on this, such as imposing geometric constraints [19, 30], training to directly predict radiance fields by using networks conditioned on image features [6, 50, 59], or constraining depth [8, 49, 60]. The first is difficult to do for complicated scenes while the second is often limited to very specific 3-view setting and not easily generalizable to unbounded scenes or scalable to more input views. The last, depth regularization, has proved to be the more widely applicable. However, it typically requires excessive expensive 3D supervision, and can produce unreliable predictions on challenging open-space scenes that produce artifacts in the final NeRF reconstruction.

To remedy this, we propose to use view-consistency distributions per-ray instead of fixed depth predictions to implement a sampling technique along the rays that implicitly regularizes the training of NeRF, as depicted by Fig. 1. Specifically, we first distill geometric information from the redundant feature representations of foundation models to reduce their dimensionality and to alleviate memory requirements, while preserving the information most likely to be consistent across views and discarding the rest. Given these high-level distilled features along with low-level color features, we compute a view-consistency metric for every point along the rays and introduce an adaptive sampling scheme that favors view-consistent points, on the assumption that they are more likely to lie on a real-world surface. Furthermore, we also introduce a depth-pushing loss to force the model to favor samples that are farther away from the camera origin, which prevents the kind of background collapse artifact [2] that frequently happens in NeRF reconstruction of real-world unbounded scenes. In effect, the proposed view-consistent sampling and the depth-pushing loss focus the NeRF reconstruction process on the part of the capture volume close to the true surface, thus providing

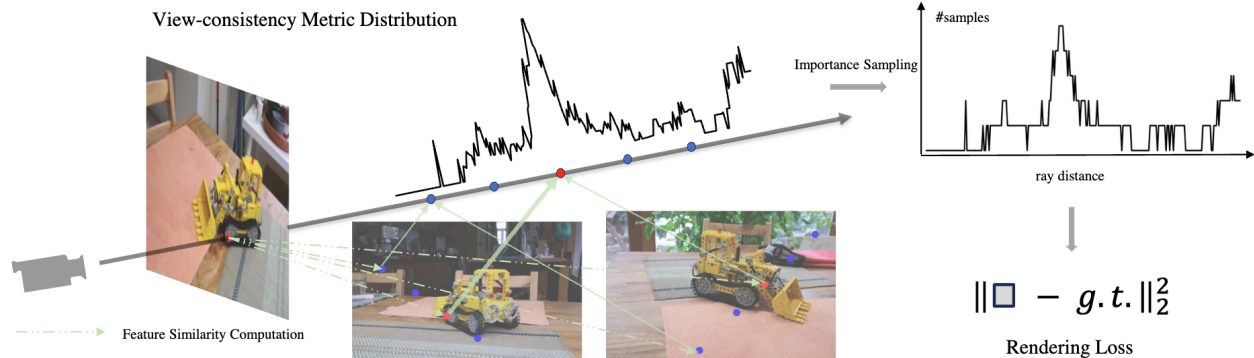


Figure 1. **View-consistent sampling.** Our central idea is to pre-compute a view-consistency distribution along rays and to perform importance sampling according to this distribution. As a result, the sampling will concentrate around **surface points** instead of **random points** in the capture volume.

implicit regularization and preventing the overfitting problem [62].

Our contribution is therefore a novel view-consistent sampling technique to implicitly regularize the training of NeRF. We show that our method is able to achieve significantly better novel view synthesis results compared to existing NeRF competitors with regularizations. Our implementation is based on open-source software and will be made publicly available.

2. Related Works

NeRF Variants. The emergence of Neural Radiance Fields (NeRF) [28] is an immediate consequence of the study on Implicit Neural Representations (INR) [14, 27, 37, 42], which laid the foundation of NeRF by introducing powerful network-based scene representation models. NeRFs use them to effectively encode 3D scene properties and trains on posed images via a volume rendering equation that differentially relates 3D scenes to 2D images.

NeRFs deliver outstanding image synthesis results but tend to be slow, sometimes requiring several days for a single scene. A number of accelerated approaches have therefore been proposed [7, 10, 29, 40], using various kinds of efficient scene representation techniques. Interestingly, not only are these approaches faster, they also tend to yield better image synthesis results. Other works have focused more directly on improving the quality of the synthesis results [1–3, 45, 62], by introducing unbounded scene representations or reducing aliasing artifacts. Nerfacto [43], introduced in the popular Nerfstudio project, combines many components of these approaches into an integrated one. Hence, we use it as the basis for implementing our own approach.

Gaussian Splatting. 3D Gaussian Splatting [17] has recently emerged as a powerful alternative to NeRFs for novel view synthesis results using an explicit point-based repre-

sentation. It is arguably better at novel-view synthesis but NeRF-based models continue to shine in many scenarios, offering unique advantages through their continuous representations. This is the case in applications such as surface reconstruction [24], 3D scene understanding [18] and inverse rendering [16]. In addition, the general regularization method we propose could be potentially used in Gaussian Splatting as well, by simply changing the point sampling method to a Gaussian placement one.

Regularizers. A straightforward approach to improving the performance of NeRFs is to incorporate geometric priors to regularize and guide the training process. To this end, many methods have been proposed. They rely on depth guidance [8, 34, 48, 49, 60], geometric constraints [19, 30, 39, 44], or pre-training on similar scenes [6, 50, 53, 56, 59]. However, these methods are all plagued by generalization issues. For depth priors, it is difficult to obtain accurate depth predictions, especially in real-world unbounded scenes. The geometry-based constraints often fail to properly refine the results in complex unbounded scenes. Prediction-based methods are mostly restricted to a 3-view setting in bounded scenes, due to the limitations of a prediction-based architecture and the limited availability of real-world unbounded scene data with 3D ground truth. Note also that many methods have been proposed for only sparse-view cases [15, 36, 38, 39, 47, 57, 61, 65], which however are restricted in denser-view settings. Recently, ReconFusion [54] has been proposed to incorporate diffusion prior into NeRF training. This method works well for indoor or bounded scenes, but for open-space scenes the performance drops drastically as the original paper shows.

Image Features. Recently, there has been tremendous progress in large-scale self-supervised pre-training using Masked image Modeling [13, 52, 64] (MIM). These new techniques yield foundation models, such as DINOv2 [31],

which encode local geometric information better than classification pretraining [55], which makes them very useful in a NeRF context. Image features that even better for image matching can be obtained [9, 35, 41, 44, 46, 58]. However the pairwise matching schemes they are mostly intended for is not the best one for handling large image collections because it does not leverage multi-image cues.

3. Methodology

We now introduce our *View-consistent Sampling* (VS-NeRF) approach for NeRF training. As our method is built on the standard NeRF framework, we first describe it briefly in Sec. 3.1. Next, we describe our approach to distill high-level image features and preserve only view-consistent information from the foundation model DINOv2 [31] in Sec. 3.2. We then introduce a sampling mechanism to exploit these features as well as color features along camera rays in Sec. 3.3. Finally, we describe the proposed depth-pushing loss as a weaker regularization to force the model to favor distant samples in in Sec. 3.4.

3.1. NeRF Basics

Scene Representation. The 3D scene is generally represented by an MLP, and optionally and additional feature grid, which encode both geometry information and view-dependent color information. Specifically, the geometry of the scene is encoded by the neural network as a function $f : \mathbb{R}^3 \rightarrow \mathbb{R}$ that maps a spatial coordinate $\mathbf{x} \in \mathbb{R}^3$ to its corresponding volume density value σ . The view-dependent color information is encoded by the network as a function $f : \mathbb{R}^3 \times \mathbb{S}^2 \rightarrow \mathbb{R}^3$ that takes a point coordinate $\mathbf{x} \in \mathbb{R}^3$ as well as a viewing direction \mathbf{d} as input and outputs the associated view-dependent color value $\mathbf{c} = (r, g, b)$.

Volume Rendering. The rendering process is of critical importance because it associates a 3D representation of the scene with 2D images, which makes the use of image reconstruction loss possible. In the NeRF literature, the most frequently used rendering technique in 3D vision tasks is known to be volume rendering. Given a ray $\mathbf{r}(t) = \mathbf{o} + t\mathbf{d}$, the volume rendering equation yields the color of one pixel in the 2D image corresponding to the ray \mathbf{r} by evaluating

$$\hat{\mathbf{C}}(\mathbf{r}) = \int_{t_n}^{t_f} \omega(t)\mathbf{c}(\mathbf{r}(t), \mathbf{d})dt, \quad (1)$$

where $\omega(t) = T(t)\sigma(\mathbf{r}(t))$ is the weight function, σ represents the volume density, \mathbf{c} represents the directional color, and $T(t) = \exp(-\int_{t_n}^t \sigma(\mathbf{r}(s))ds)$ represents the transparency function.

In practice, this integral is evaluated by sampling the ray in discrete locations, which is of vital importance depending on the sampling scheme [2]. NeRF volume rendering is then

performed by accumulating color values from S samples $(t_i)_{1 \leq i \leq S}$ along a ray \mathbf{r} . This yields

$$\hat{\mathbf{C}}(\mathbf{r}) = \sum_{i=1}^S T_i(1 - \exp(-\sigma_i \delta_i))\mathbf{c}_i, \quad T_i = \exp\left(-\sum_{j=1}^{i-1} \sigma_j \delta_j\right) \quad (2)$$

where $\delta_i = t_{i+1} - t_i$ is the distance between two consecutive samples.

Loss Function. Given the estimated color $\hat{\mathbf{C}}(\mathbf{r})$ of Eq. (2), let $\mathbf{C}(\mathbf{r})$ be the corresponding pixel true color. Using these notations, we can define an MSE loss

$$\mathcal{L}_{color} = \frac{1}{|\mathcal{B}|} \sum_{\mathbf{r} \in \mathcal{B}} \|\hat{\mathbf{C}}(\mathbf{r}) - \mathbf{C}(\mathbf{r})\|^2, \quad (3)$$

where \mathcal{B} denotes a randomly chosen batch of rays and $|\mathcal{B}|$ denotes the batch size. The weights of the NeRF scene representation network are computed by minimizing this loss, using a different batch of rays at each iteration.

3.2. Distillation of Geometric Information

To form meaningful view-consistent statistics for adaptive sampling, a good representation of images in the context of multi-view captures is critical. In this paper, we propose to use foundation models that provide powerful general-purpose visual features, e.g. DINOv2 [31], for extracting such high-level representations containing crucial context information. Note that there are alternatives to DINOv2 such as features from diffusion models [25], which we found to deliver similar results. Since diffusion models are slower in inference time, we opted to use DINOv2. However, there are two main hurdles in utilizing the features from foundation models. Firstly, as general-purpose features, the output of a foundation model encodes image information in many different aspects that are useful in different tasks. In the NeRF setting, we are particularly interested in geometric information that can be expected to be similar across multi-view images of the same scene. Secondly, the dimensionality of features from foundation models is in general very high, e.g. 384 in DINOv2, resulting in prohibitively large memory consumption in sampling.

In this paper, we propose to resolve the issues by distilling geometric information from the foundational features. Note that we use the term *distillation* in a different way than in *Feature Field Distillation* papers, such as [21], which focuses on lifting 2D features to a 3D representation. We distill features by extracting geometric information from redundant high-dimensional image features. Inspired by [25], we use a very lightweight Resnet bottleneck block [12] to project the high-dimensional features to a lower dimension for distillation. To supervise the distillation process,

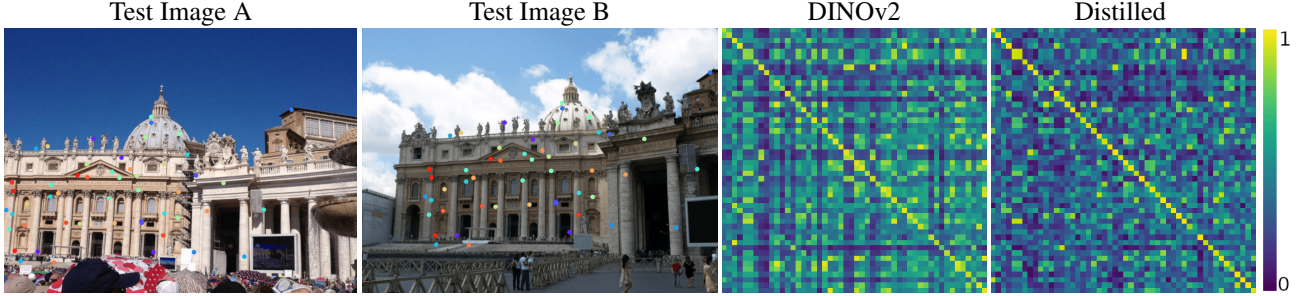


Figure 2. Visualization of the feature distillation process. For the two test images from Megadepth dataset [23], we first randomly generate 50 ground truth correspondences (same as in the training process), shown as colored dots, and then extract vanilla DINOv2 features (384 dimension) and the proposed distilled DINOv2 features (32 dimension) at these locations. We compute the feature similarities across the two views and show the resulting similarity matrices on the right, where an optimal correspondence should give the identity matrix.

we adopt the Megadepth dataset [23] which provides 3D ground truth and is prevalently used in geometric matching tasks.

Training of Distillation Process. We adopt a very simple strategy for training. Specifically, in the training phase, we freeze the foundation model and only update the parameters in the Resnet bottleneck block. This leads to a much smaller number of training parameters and also requires much less data. We randomly choose 50000 pairs of images from Megadepth to train. For each image pair, we use the ground truth depth map to randomly generate 50 corresponding points, and extract the distilled features at the point locations on the image pairs. We then supervise the network using a symmetric cross entropy loss, in the same fashion as CLIP [33], to make extracted features in corresponding locations as close as possible while still being distinctive from other features. A visualization of the distillation process can be found in Fig. 2. As a result, in our experiments we can reduce the feature dimensionality by a factor of around 10, e.g. 384 from DINOv2 to 32, without compromising on useful geometric information. Please refer to the ablation studies in Sec. 4.2 for the discussion of optimal dimensionality in NeRF settings.

3.3. View-Consistent Sampling

In the original NeRF and most NeRF variants, the volume rendering of Eq. (2) is typically achieved using naive sampling strategies such as uniform, stratified, or linear disparity sampling. Hence, there is no prior in the sampling process and hence no regularization while learning the radiance and density fields. When there are abundant input views, this is usually not an issue but it can result in unwanted artifacts with a smaller set of input images.

VS-NeRF remedies this by making the sampling adaptive based on a prior: it samples more densely the 3D locations whose projections have view-consistent features because they are more likely to correspond to 3D surface

points. This requires both a view-consistency metric and an adaptive sampling scheme based on that metric, which we describe in Sections 3.3.1 and 3.3.2, respectively. A graphical visualization of the proposed view-consistent sampling technique can be seen in Fig. 1.

Sampling Setup. We assume that we have a collection of N posed images $\{\mathbf{I}_i\}_{i=1}^N$, from which we generate image feature representations $\{\mathbf{F}_i\}_{i=1}^N$. As in NeRF and most of its variants, the training is performed by repeatedly sampling a batch of rays. For each ray \mathbf{r} , we initially need to place pre-samples along the ray $(t_i)_{1 \leq i \leq M}^{pre}$, to obtain M points $\{\mathbf{p}_i\}_{i=1}^M$. Note that these pre-samples are different from the initial samples in NeRF, as pre-samples are for computing view-consistency statistics only and will not be used to compute losses. The pre-samples are generated uniformly within a distance, but after a fixed threshold the step sizes will increase with each sample due to scene contraction. This strategy is the same as the initial sampling strategy in Nerfacto [43] and we refer to the original paper for details.

3.3.1. Computation of View-Consistency Metric

Features from Projections. As shown in Fig. 3, the feature representation at the pixel location where the ray comes from is denoted as reference feature \mathbf{f}_r . For each pre-sample point \mathbf{p}_i , we can project it onto an arbitrary view v_j . If the point \mathbf{p}_i is visible to v_j , then naturally by interpolating over the feature representation \mathbf{F}_j , we can obtain the projection feature \mathbf{f}_{ij} . Due to limited field-of-view (FOV) of cameras, there is a varying number of views that a point \mathbf{p}_i can be projected onto. We denote the set of views that a point \mathbf{p}_i can be projected onto as V_i , and $|V_i|$ as its cardinality.

Normalized Similarity Measure. In this paper, we jointly use high-level distilled features, and plain normalized RGB values as low-level color features. Please see the



Figure 3. Visualization of the effectiveness of the view-consistency metric on the BONSAI scene from the MipNeRF360 dataset. As shown, we shoot a ray from the reference point in the leftmost image, compute the view-consistency metric distribution along the ray, and reproject the peak point in the distribution onto other views. The projections of the peak are consistent and correspond to a surface point.

ablation study in Sec. 4.2 to understand their respective effects. However, the two kinds of features are defined in different metric spaces. That is to say, while Euclidean distances can be used for measuring discrepancies among color features, cosine similarities are most frequently used as a distance measure of features from pre-trained models such as DINOv2. In this paper, we use a normalizing strategy to convert the measures among features to binary numbers, be it color feature or distilled feature. In particular, along an arbitrary ray \mathbf{r} , we first compute the measures between the reference feature and projection features from all sampled points $\{m(\mathbf{f}_r, \mathbf{f}_{ij}) \mid j \in V_i\}$, be it Euclidean distances or cosine similarities. We then normalize the set of measures m based on its variance $\sigma_m = \sqrt{\frac{1}{N_m} \sum_{i=1}^{N_m} m_i^2}$, and take the negative if the measure is Euclidean distance to align distance with similarity. Thus, we have defined the normalized similarity measure $\{m_n(\mathbf{f}_r, \mathbf{f}_{ij}) \mid j \in V_i\}$.

View-consistency Metric. Given the normalized similarity measure $\{m_n(\mathbf{f}_r, \mathbf{f}_{ij}) \mid j \in V_i\}$, we assume its values follow a normal distribution and we experimentally determine a reasonable threshold δ accordingly. The view-consistency metric of point \mathbf{p}_i along the ray is computed as:

$$s_i = \frac{1}{|V_i|} \sum_{j \in V_i} \mathbb{1}\{m_n(\mathbf{f}_r^c, \mathbf{f}_{ij}^c) > \delta \wedge m_n(\mathbf{f}_r^d, \mathbf{f}_{ij}^d) > \delta\}, \quad (4)$$

where $\mathbb{1}$ denotes the indicator function, superscripts c and d denote *color* and *distilled* in projection features respectively. Intuitively, Eq. (4) measures the average view consistency over the views the point can be projected onto. Although occlusions may hinder the effectiveness of this metric, statistically the score is still prominent for surface points. A visualization of the computed view-consistency metrics along a ray using real data can be seen in Fig. 3.

3.3.2. Adaptive Sampling Scheme

Given the view-consistency metric of Eq. (4), implementing view-consistent sampling becomes straightforward. After computing the metric for each pre-sampled point along

the ray, we perform importance sampling based on the distribution along the ray. Our rationale is that this view-consistency distribution is concentrated around the surface point, thus importance sampling from the distribution is the logical way to improve it.

In our implementation, we use the Probability Distribution Function (PDF) sampler from Nerfstudio [43] to perform importance sampling, which generate samples that match a distribution. Specifically, as illustrated by Fig. 1, we first compute view-consistency metrics from pre-samples $(t_i)_{1 \leq i \leq M}$ along the ray. The PDF sampler will probabilistically sample the bins between consecutive pre-sample points, such that the distribution of number of samples in each bin will match the view-consistency distribution, which gives the true samples $(t_i)_{1 \leq i \leq S}$ to compute losses as in Eq. (2).

3.4. Depth-pushing Loss

In NeRF, the background of the scene is generally harder to reconstruct than foreground objects, typically because parts of the background may only be seen in very few views. To complement our adaptive sampling scheme, we introduce a depth-pushing loss which favors distant samples along the ray and provides a regularization to prevent background collapse. This shares a similar idea to prioritizing sampling distant points [30, 57]. We write

$$\mathcal{L}_{depth} = -\frac{1}{|\mathcal{B}|} \sum_{\mathbf{r} \in \mathcal{B}} \log(d(\mathbf{r}) + \varepsilon) \quad (5)$$

$$\text{where } d(\mathbf{r}) = \sum_{i=1}^S T_i (1 - \exp(-\sigma_i \delta_i)) t_i, \quad (6)$$

where ε is a small constant that stabilizes the logarithm function near 0 and $d(\mathbf{r})$ is the expected depth along the ray. Its simple form makes it easy to integrate into the NeRF framework by adding it to the color loss of Eq. (3).

4. Experimental Results

In this section, we demonstrate the effectiveness of our VS-NeRF approach, which includes a discussion of experimental settings and implementation details; evaluation results



Figure 4. We show comparisons of VS-NeRF to the main competitors and the corresponding ground truth images from held-out test views. The scenes are, from the top down: BICYCLE with 60 training views, STUMP with 110 training views, COUNTER with 70 training views from the Mip-NeRF360 dataset and FRANCIS with 70 training views from Tanks&Temples. The '+' prefix indicates the included additional component to Nerfacto.

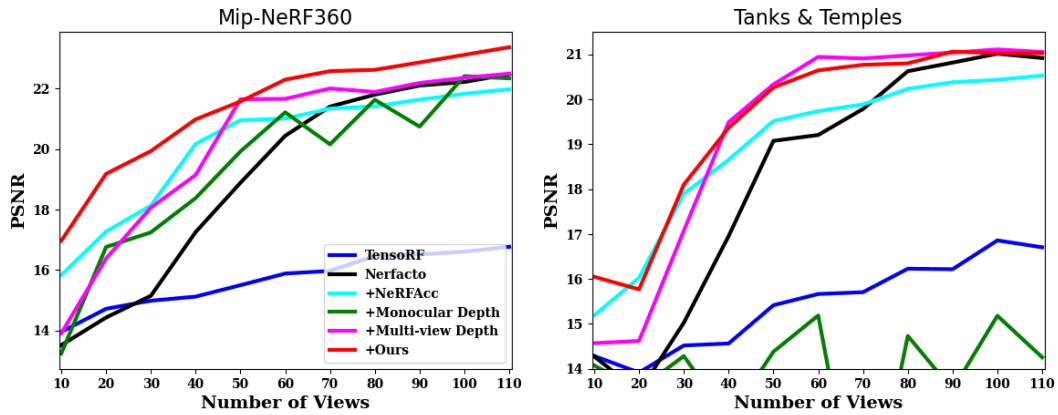


Figure 5. We show performances of VS-NeRF and competitors with increasing number of views over Mip-NeRF360 dataset and Tanks&Temples, in terms of PSNR values. The '+' prefix indicates the included additional component to Nerfacto.

on benchmark datasets and comparison with previous work; and an ablation study with respect to the major components in VS-NeRF.

Implementation Details. Our implementation of VS-NeRF is built upon the Nerfacto method from the Nerfstudio project [43]. It incorporates many published methods

Dataset Method / Metric	Mip-NeRF360				Tanks&Temples			
	PSNR \uparrow	SSIM \uparrow	LPIPS \downarrow	Train	PSNR \uparrow	SSIM \uparrow	LPIPS \downarrow	Train
TensoRF	15.68	0.455	0.658	25m29s	15.46	0.609	0.566	29m07s
Nerfacto	19.05	0.549	0.495	11m37s	18.29	0.688	0.422	11m16s
+NeRFacc	20.14	0.580	0.480	12m18s	18.95	0.691	0.431	12m07s
+Monocular Depth	19.45	0.549	0.488	11m55s	13.81	0.451	0.632	12m20s
+Multi-view Depth	20.15	0.578	0.465	12m24s	19.28	0.706	0.397	12m10s
+Ours	21.40	0.625	0.400	38m44s	19.45	0.714	0.373	39m05s

Table 1. Quantitative evaluation of our method compared to previous work, computed over two datasets. The '+' prefix indicates the included additional component to Nerfacto.

that have been found to work well for real data, such as Mip-NeRF360 [2], InstantNGP [29], and NeRF-W [26]. We simply replace Nerfacto’s sampling scheme by ours and add our depth-pushing loss and keep all other settings the same. Notably, the Nerfacto proposal network sampling scheme, from Mip-NeRF360 [2], is also left unchanged. This ensures that any difference in performance is attributable to our regularization scheme. We turn off the camera optimization for both VS-NeRF and Nerfacto, since we observed a negative impact on datasets with accurate camera parameters.

To reduce the time cost, we only activate the proposed view-consistent sampling technique in the first 5000 iterations out of 30000 in total, which is when the regularization of the geometry is the most needed. Empirically, the threshold δ in Eq. (4) is set to 0.4, the weight of depth-pushing loss is set to 0.0001, and the ε in the depth pushing loss as in Eq. (5) is set to 0.01.

Baselines. Since our implementation is based on **Nerfacto** [43], we treat it as a baseline to demonstrate the positive impact of our adaptive sampling scheme and depth-pushing loss. We also use **TensoRF** [7] as another baseline that features efficient training. In addition we also compare against InstantNGP [29] from the Nerfstudio project. The most prominent difference between InstantNGP [29] and **Nerfacto** [43] is the **NeRFacc** [22] efficient sampling scheme, whose name we will use to refer to this method. We also incorporated our sampling method into MipNeRF360 [2], which is significantly slower but yields better performance due to its anti-aliasing design.

Regarding depth regularizations, we compare against both monocular and multi-view methods, using the depth-nerfacto method, again from Nerfstudio project. To test the method with **Monocular Depth** regularization, we use ZoeDepth [4] to predict pseudo depth and apply depth-ranking loss from SparseNeRF [49]. To test the method with **Multi-view Depth** regularization, we use the state-of-the-art MVFormer++ [5] to provide depth estimations from correlating with adjacent 9 views, along with the depth loss from DS-NeRF [8].

Additionally, we also apply our method to **Mip-NeRF360** [2] and compare with **3DGS** [17].

Datasets and Metrics. We use two benchmark datasets for our main evaluation, first the 9 full scenes from Mip-NeRF360 [2] and second all 8 scenes from the INTERMEDIATE official test set in Tanks & Temples dataset [20]. The scenes in the two datasets contain both a complex central object or area and a detailed background, and cover both bounded indoor scenes and large unbounded outdoor environments, making them challenging for NeRF methods. We use the same hyperparameter configuration for all experiments.

In order to study the effect of the number of available views on the reconstruction quality, we subsample between 10 to 110 images per scene, 110 being the size of the smallest image set in our datasets. To this end, for each scene, we first evenly sample 10 images as an evaluation set and then sample evenly the remaining views. In ablation study, we use 50 views for all scenes, as it is a reasonable number for practical usage and we observed that the need for regularization is highest as the number of views decreases.

Following the usual convention, we report quantitative results based on PSNR, SSIM [51], and LPIPS [63], along with the training time in minutes as measured on a single NVIDIA A100 80GB GPU.

4.1. Comparative Results

Efficient NeRF Variants. We report our comparative results with efficient NeRF variants on our two datasets as a function of the number of training views being used in Fig. 5. We provide evaluation metrics averaged over all different scenes with different training view numbers in Tab. 1 and qualitative results in Fig. 4. VS-NeRF clearly outperforms all baselines in terms of novel view synthesis quality on Mip-NeRF360. On Tanks&Temples, multi-view depth regularization is on par with our method when views are dense, but our method performs better in sparser cases. Crucially, our method significantly outperforms Nerfacto, upon which our implementation is based, which conclusively demonstrates the effectiveness of our view-consistent

	PSNR \uparrow	SSIM \uparrow	LPIPS \downarrow	Train
A) Base Method Nerfacto	18.88	0.544	0.503	13m20s
B) Base + VS (Sec. 3.3)	19.34	0.574	0.456	38m54s
C) Base + DL (Sec. 3.4)	19.10	0.552	0.481	11m27s
D) Base + VS (Only Color Feature (Eq. (4))) + DL	19.42	0.571	0.454	32m51s
E) Base + VS (Only Distilled Feature (Eq. (4))) + DL	19.96	0.584	0.434	38m11s
F) Base + VS (Distilled Feature Dimension as 16 (Sec. 3.2)) + DL	20.04	0.587	0.432	39m22s
G) Base + VS (Distilled Feature Dimension as 64 (Sec. 3.2)) + DL	21.65	0.633	0.401	48m22s
Base + VS + DL (Our Complete Model)	21.57	0.631	0.400	38m44s

Table 2. Ablation study in which we remove or replace the major components in our method to measure their effect on the Mip-NeRF360 dataset with 50 training views. The two major components are VS: *View-consistent Sampling* and DL: *Depth-pushing Loss*.

sampling and depth-pushing loss. Note that NeRFacc also yields considerable improvement over Nerfacto when available views are sparser but its relative performance drops when the number of views increases, which is not the case for our approach. TensorRF seems to struggle most, presumably due to the limitations of tensor-based scene representation in complex and unbounded scenes. We also compare against two different depth-based regularizers, a monocular one using MVSformer++ and a multi-view one using ZoeDepth. Monocular depth estimation produces many artifacts and results in unstable performance, especially on Tanks&Temples. This is largely because monocular depth is only a pseudo depth that may not be consistent across views. The multi-view depth regularization performs significantly better than the monocular one and consistently improves over Nerfacto. However, in challenging scenes with few available views it may produce unreliable depth estimations. In contrast, our method samples from a view-consistency distribution and is more robust as can be seen in results on Mip-NeRF360 dataset.

Dataset Method / Metric	Mip-NeRF360			
	PSNR \uparrow	SSIM \uparrow	LPIPS \downarrow	Train
Mip-NeRF360	22.54	0.642	0.347	29h22m
Mip-NeRF360+Ours	23.37	0.676	0.316	32h17m
3DGS	23.53	0.716	0.278	27m38s

Table 3. Additional results comparing to Mip-NeRF360 and 3D Gaussian Splatting.

Slower NeRF Variant. In the above experiments, we compared against some of the most efficient NeRF variants. We also apply our method to slower Mip-NeRF360 and report our results in Tab. 3. Our sampling method clearly brings about an improvement.

Gaussian Splatting. For completeness, we also compare with 3D Gaussian Splatting [17], which has emerged as a powerful alternative to NeRF for novel view synthesis using an explicit point-based representation. To this end, we use the Splatfacto method from Nerfstudio [43]. As can be seen in Tab. 3, 3DGS yields the best performance of all for view synthesis. However, as discussed in Sec. 2, there are many applications, from to surface reconstruction [24] and

3D scene understanding [18] to inverse rendering [16], for which NeRF-like representations are more appropriate and yield better results than 3DGS. Thus, our results remain entirely relevant to these.

4.2. Ablation Study

We perform an ablation study of the two novel components of our approach, i.e. the *View-consistent Sampling* (VS) and the *Depth-pushing Loss* (DL). For simplicity, the experiment is conducted with a moderate 50-view setting for subsampling the scenes on Mip-NeRF360 dataset. The results are presented in Tab. 2. The first three rows of the table show that each component, VS or DL, brings an improvement when used separately. Comparing to our complete model in ie last row, it shows that they work best when used jointly. Regarding the features used to compute the view-consistency metric, distilled DINOv2 features are more powerful than color feature when used independently, but the best performance is achieved by combining them, as in Eq. (4). The dimensionality of the distilled features is also investigated here. We see that reducing the dimensionality to 16 or increasing it to 64 will degrade performance. Thus, we opt to use 32 as the dimensionality of distilled features in our implementation.

5. Conclusion

We have proposed a novel view-consistent sampling technique as a regularization for the training of NeRF. The core idea is to combine high-level and low-level features to compute view-consistency metrics, and use it as a prior distribution to sample on the ray. To mitigate the background collapse problem, we also propose a depth-pushing loss, which imposes a weaker regularization to favor distant samples on the ray. Extensive experiments on public datasets have demonstrated the effectiveness of the proposed method. Note that our method typically introduces more computational overhead than NeRF or Gaussian Splatting. In future work, we will look into more efficient implementations and extending our regularization method to Gaussian Splatting as well.

References

- [1] J. Barron, B. Mildenhall, M. Tancik, P. Hedman, R. Martin-Brualla, and P. Srinivasan. Mip-Nerf: A Multiscale Representation for Anti-Aliasing Neural Radiance Fields. In *International Conference on Computer Vision*, pages 5855–5864, 2021. 2
- [2] J. Barron, B. Mildenhall, D. Verbin, P. P. Srinivasan, and P. Hedman. Mip-Nerf 360: Unbounded Anti-Aliased Neural Radiance Fields. In *Conference on Computer Vision and Pattern Recognition*, 2022. 1, 3, 7
- [3] Jonathan T Barron, Ben Mildenhall, Dor Verbin, Pratul P Srinivasan, and Peter Hedman. Zip-nerf: Anti-aliased grid-based neural radiance fields. In *Proceedings of the IEEE/CVF International Conference on Computer Vision*, pages 19697–19705, 2023. 2
- [4] Shariq Farooq Bhat, Reiner Birkl, Diana Wofk, Peter Wonka, and Matthias Müller. Zoedepth: Zero-shot transfer by combining relative and metric depth. *arXiv preprint arXiv:2302.12288*, 2023. 7
- [5] Chenjie Cao, Xinlin Ren, and Yanwei Fu. Mvsformer++: Revealing the devil in transformer’s details for multi-view stereo. *arXiv preprint arXiv:2401.11673*, 2024. 7
- [6] Anpei Chen, Zexiang Xu, Fuqiang Zhao, Xiaoshuai Zhang, Fanbo Xiang, Jingyi Yu, and Hao Su. Mvsnerf: Fast generalizable radiance field reconstruction from multi-view stereo. In *Proceedings of the IEEE/CVF International Conference on Computer Vision*, pages 14124–14133, 2021. 1, 2
- [7] A. Chen, Z. Xu, A. Geiger, J. Yu, and H. Su. Tensorf: Tensorial Radiance Fields. In *European Conference on Computer Vision*, pages 333–350, 2022. 2, 7
- [8] Kangle Deng, Andrew Liu, Jun-Yan Zhu, and Deva Ramanan. Depth-supervised nerf: Fewer views and faster training for free. In *Proceedings of the IEEE/CVF Conference on Computer Vision and Pattern Recognition*, pages 12882–12891, 2022. 1, 2, 7
- [9] Johan Edstedt, Qiyu Sun, Georg Bökman, Mårten Wadenbäck, and Michael Felsberg. Roma: Revisiting robust losses for dense feature matching. *arXiv preprint arXiv:2305.15404*, 2023. 3
- [10] S. Fridovich-Keil, A. Yu, M. Tancik, Q. Chen, B. Recht, and A. Kanazawa. Plenoxels: Radiance fields without neural networks. In *Conference on Computer Vision and Pattern Recognition*, pages 5501–5510, 2022. 2
- [11] R. Hartley and A. Zisserman. *Multiple View Geometry in Computer Vision*. Cambridge University Press, 2000. 1
- [12] K. He, X. Zhang, S. Ren, and J. Sun. Deep Residual Learning for Image Recognition. In *Conference on Computer Vision and Pattern Recognition*, pages 770–778, 2016. 3
- [13] K. He, X. Chen, S. Xie, Y. Li, P. Dollár, and R. Girshick. Masked Autoencoders Are Scalable Vision Learners. In *Conference on Computer Vision and Pattern Recognition*, pages 16000–16009, 2022. 2
- [14] Amir Hertz, Or Perel, Raja Giryes, Olga Sorkine-Hornung, and Daniel Cohen-Or. Sape: Spatially-adaptive progressive encoding for neural optimization. *Advances in Neural Information Processing Systems*, 34:8820–8832, 2021. 2
- [15] Ajay Jain, Matthew Tancik, and Pieter Abbeel. Putting nerf on a diet: Semantically consistent few-shot view synthesis. In *Proceedings of the IEEE/CVF International Conference on Computer Vision*, pages 5885–5894, 2021. 2
- [16] Haian Jin, Isabella Liu, Peijia Xu, Xiaoshuai Zhang, Songfang Han, Sai Bi, Xiaowei Zhou, Zexiang Xu, and Hao Su. Tensor: Tensorial inverse rendering. In *Proceedings of the IEEE/CVF Conference on Computer Vision and Pattern Recognition*, pages 165–174, 2023. 2, 8
- [17] B. Kerbl, G. Kopanas, T. Leimkühler, and G. Drettakis. 3D Gaussian Splatting for Real-Time Radiance Field Rendering. *ACM Transactions on Graphics*, 42(4), 2023. 2, 7, 8
- [18] J. Kerr, C. Kim, K. Goldberg, A. Kanazawa, and M. Tancik. LERF: Language Embedded Radiance Fields. In *International Conference on Computer Vision*, 2023. 2, 8
- [19] Mijeong Kim, Seonguk Seo, and Bohyung Han. Infonerf: Ray entropy minimization for few-shot neural volume rendering. In *Proceedings of the IEEE/CVF Conference on Computer Vision and Pattern Recognition*, pages 12912–12921, 2022. 1, 2
- [20] Arno Knapitsch, Jaesik Park, Qian-Yi Zhou, and Vladlen Koltun. Tanks and temples: Benchmarking large-scale scene reconstruction. *ACM Transactions on Graphics (ToG)*, 36(4):1–13, 2017. 7
- [21] S. Kobayashi, E. Matsumoto, and V. Sitzmann. Decomposing NeRF for Editing via Feature Field Distillation. In *Advances in Neural Information Processing Systems*, 2022. 3
- [22] Ruilong Li, Hang Gao, Matthew Tancik, and Angjoo Kanazawa. Nerfacc: Efficient sampling accelerates nerfs. In *Proceedings of the IEEE/CVF International Conference on Computer Vision*, pages 18537–18546, 2023. 7
- [23] Zhengqi Li and Noah Snavely. Megadepth: Learning single-view depth prediction from internet photos. In *Proceedings of the IEEE conference on computer vision and pattern recognition*, pages 2041–2050, 2018. 4
- [24] Z. Li, T. Müller, A. Evans, R. Taylor, M. Unberath, M. Liu, and C. Lin. Neuralangelo: High-Fidelity Neural Surface Reconstruction. In *Conference on Computer Vision and Pattern Recognition*, 2023. 2, 8
- [25] Grace Luo, Lisa Dunlap, Dong Huk Park, Aleksander Holynski, and Trevor Darrell. Diffusion hyperfeatures: Searching through time and space for semantic correspondence. *Advances in Neural Information Processing Systems*, 36, 2024. 3
- [26] Ricardo Martin-Brualla, Noha Radwan, Mehdi SM Sajjadi, Jonathan T Barron, Alexey Dosovitskiy, and Daniel Duckworth. Nerf in the wild: Neural radiance fields for unconstrained photo collections. In *Proceedings of the IEEE/CVF Conference on Computer Vision and Pattern Recognition*, pages 7210–7219, 2021. 7
- [27] Ishit Mehta, Michaël Gharbi, Connelly Barnes, Eli Shechtman, Ravi Ramamoorthi, and Manmohan Chandraker. Modulated periodic activations for generalizable local functional representations. In *Proceedings of the IEEE/CVF International Conference on Computer Vision*, pages 14214–14223, 2021. 2

- [28] Ben Mildenhall, S. P. P., M. Tancik, J. T. Barron, R. Ramamoorthi, and R. Ng. NeRF: Representing Scenes as Neural Radiance Fields for View Synthesis. In *European Conference on Computer Vision*, 2020. 1, 2
- [29] Thomas Müller, Alex Evans, Christoph Schied, and Alexander Keller. Instant neural graphics primitives with a multiresolution hash encoding. *ACM Transactions on Graphics (ToG)*, 41(4):1–15, 2022. 2, 7
- [30] Michael Niemeyer, Jonathan T Barron, Ben Mildenhall, Mehdi SM Sajjadi, Andreas Geiger, and Noha Radwan. Regnerf: Regularizing neural radiance fields for view synthesis from sparse inputs. In *Proceedings of the IEEE/CVF Conference on Computer Vision and Pattern Recognition*, pages 5480–5490, 2022. 1, 2, 5
- [31] M. Oquab, T. Darcet, T. Moutakanni, H. Vo, M. Szafraniec, V. Khalidov, P. Fernandez, D. Haziza, F. Massa, A. El-Nouby, R. Howes, P. Huang, H. Xu, V. Sharma, S. Li, W. Galuba, M. Rabbat, M. Assran, N. Ballas, G. Synnaeve, I. Misra, H. Jegou, J. Mairal, P. Labatut, A. Joulin, and P. Bojanowski. DINOv2: Learning Robust Visual Features Without Supervision. In *arXiv Preprint*, 2023. 2, 3
- [32] E. Prados and O. Faugeras. Shape from Shading: A Well-Posed Problem? In *Conference on Computer Vision and Pattern Recognition*, 2005. 1
- [33] A. Radford, J. Kim, C. Hallacy, A. Ramesh, G. Goh, S. Agarwal, G. Sastry, A. Askell, P. Mishkin, J. Clark, et al. Learning transferable visual models from natural language supervision. In *International Conference on Machine Learning*. PMLR, 2021. 4
- [34] Barbara Roessle, Jonathan T Barron, Ben Mildenhall, Pratul P Srinivasan, and Matthias Nießner. Dense depth priors for neural radiance fields from sparse input views. In *Proceedings of the IEEE/CVF Conference on Computer Vision and Pattern Recognition*, pages 12892–12901, 2022. 2
- [35] P.E. Sarlin, D. DeTone, T. Malisiewicz, and A. Rabinovich. Superglue: Learning Feature Matching with Graph Neural Networks. In *Conference on Computer Vision and Pattern Recognition*, 2020. 3
- [36] Ruoxi Shi, Xinyue Wei, Cheng Wang, and Hao Su. Zerorf: Fast sparse view 360deg reconstruction with zero pretraining. In *Proceedings of the IEEE/CVF Conference on Computer Vision and Pattern Recognition*, pages 21114–21124, 2024. 2
- [37] V. Sitzmann, J. Martel, A. Bergman, D. Lindell, and G. Wetzstein. Implicit Neural Representations with Periodic Activation Functions. In *Advances in Neural Information Processing Systems*, 2020. 2
- [38] Nagabhushan Somraj and Rajiv Soundararajan. Vip-nerf: Visibility prior for sparse input neural radiance fields. In *ACM SIGGRAPH 2023 Conference Proceedings*, pages 1–11, 2023. 2
- [39] Nagabhushan Somraj, Adithyan Karanayil, and Rajiv Soundararajan. Simplenerf: Regularizing sparse input neural radiance fields with simpler solutions. In *SIGGRAPH Asia 2023 Conference Papers*, pages 1–11, 2023. 2
- [40] C. Sun, M. Sun, and H. Chen. Direct voxel grid optimization: Super-fast convergence for radiance fields reconstruction. In *Conference on Computer Vision and Pattern Recognition*, pages 5459–5469, 2022. 2
- [41] J. Sun, Z. Shen, Y. Wang, H. Bao, and X. Zhou. LoFTR: Detector-Free Local Feature Matching with Transformers. In *Conference on Computer Vision and Pattern Recognition*, 2021. 3
- [42] M. Tancik, P. Srinivasan, B. Mildenhall, S. Fridovich-Keil, N. Raghavan, U. Singhal, R. Ramamoorthi, J. Barron, and R. Ng. Fourier Features Let Networks Learn High Frequency Functions in Low Dimensional Domains. In *Advances in Neural Information Processing Systems*, 2020. 2
- [43] M. Tancik, E. Weber, E. Ng, R. Li, B. Yi, J. Kerr, T. Wang, A. Kristoffersen, J. Austin, K. Salahi, A. Ahuja, D. McAllister, and A. Kanazawa. Nerfstudio: A Modular Framework for Neural Radiance Field Development. In *ACM SIGGRAPH*, 2023. 2, 4, 5, 6, 7, 8
- [44] Prune Truong, Marie-Julie Rakotosaona, Fabian Manhardt, and Federico Tombari. Sparf: Neural radiance fields from sparse and noisy poses. In *Proceedings of the IEEE/CVF Conference on Computer Vision and Pattern Recognition*, pages 4190–4200, 2023. 2, 3
- [45] Haithem Turki, Michael Zollhöfer, Christian Richardt, and Deva Ramanan. Pynerf: Pyramidal neural radiance fields. *Advances in Neural Information Processing Systems*, 36, 2024. 2
- [46] M. Tyszkiewicz, P. Fua, and E. Trulls. DISK: Learning Local Features with Policy Gradient. In *Advances in Neural Information Processing Systems*, 2020. 3
- [47] Mikaela Angelina Uy, Ricardo Martin-Brualla, Leonidas Guibas, and Ke Li. Scade: Nerfs from space carving with ambiguity-aware depth estimates. In *Proceedings of the IEEE/CVF Conference on Computer Vision and Pattern Recognition*, pages 16518–16527, 2023. 2
- [48] Chen Wang, Jiadai Sun, Lina Liu, Chenming Wu, Zhelun Shen, Dayan Wu, Yuchao Dai, and Liangjun Zhang. Digging into depth priors for outdoor neural radiance fields. In *Proceedings of the 31st ACM International Conference on Multimedia*, pages 1221–1230, 2023. 2
- [49] Guangcong Wang, Zhaoxi Chen, Chen Change Loy, and Ziwei Liu. Sparsenerf: Distilling depth ranking for few-shot novel view synthesis. In *Proceedings of the IEEE/CVF International Conference on Computer Vision*, pages 9065–9076, 2023. 1, 2, 7
- [50] Qianqian Wang, Zhicheng Wang, Kyle Genova, Pratul P Srinivasan, Howard Zhou, Jonathan T Barron, Ricardo Martin-Brualla, Noah Snavely, and Thomas Funkhouser. Ibrnet: Learning multi-view image-based rendering. In *Proceedings of the IEEE/CVF Conference on Computer Vision and Pattern Recognition*, pages 4690–4699, 2021. 1, 2
- [51] Zhou Wang, Alan C Bovik, Hamid R Sheikh, and Eero P Simoncelli. Image quality assessment: from error visibility to structural similarity. *IEEE transactions on image processing*, 13(4):600–612, 2004. 7
- [52] Chen Wei, Haoqi Fan, Saining Xie, Chao-Yuan Wu, Alan Yuille, and Christoph Feichtenhofer. Masked feature prediction for self-supervised visual pre-training. In *Proceedings of the IEEE/CVF Conference on Computer Vision and Pattern Recognition*, pages 14668–14678, 2022. 2

- [53] Haoyu Wu, Alexandros Graikos, and Dimitris Samaras. Svolsdf: Sparse multi-view stereo regularization of neural implicit surfaces. In *Proceedings of the IEEE/CVF International Conference on Computer Vision*, pages 3556–3568, 2023. [2](#)
- [54] Rundi Wu, Ben Mildenhall, Philipp Henzler, Keunhong Park, Ruiqi Gao, Daniel Watson, Pratul P Srinivasan, Dor Verbin, Jonathan T Barron, Ben Poole, et al. Reconfusion: 3d reconstruction with diffusion priors. In *Proceedings of the IEEE/CVF Conference on Computer Vision and Pattern Recognition*, pages 21551–21561, 2024. [2](#)
- [55] Zhenda Xie, Zigang Geng, Jingcheng Hu, Zheng Zhang, Han Hu, and Yue Cao. Revealing the dark secrets of masked image modeling. In *Proceedings of the IEEE/CVF conference on computer vision and pattern recognition*, pages 14475–14485, 2023. [3](#)
- [56] Luoyuan Xu, Tao Guan, Yuesong Wang, Wenkai Liu, Zhaojie Zeng, Junle Wang, and Wei Yang. C2f2neus: Cascade cost frustum fusion for high fidelity and generalizable neural surface reconstruction. In *Proceedings of the IEEE/CVF International Conference on Computer Vision*, pages 18291–18301, 2023. [2](#)
- [57] Jiawei Yang, Marco Pavone, and Yue Wang. Freenerf: Improving few-shot neural rendering with free frequency regularization. In *Proceedings of the IEEE/CVF conference on computer vision and pattern recognition*, pages 8254–8263, 2023. [2](#), [5](#)
- [58] K. M. Yi, E. Trulls, V. Lepetit, and P. Fua. LIFT: Learned Invariant Feature Transform. In *European Conference on Computer Vision*, 2016. [3](#)
- [59] Alex Yu, Vickie Ye, Matthew Tancik, and Angjoo Kanazawa. pixelnerf: Neural radiance fields from one or few images. In *Proceedings of the IEEE/CVF Conference on Computer Vision and Pattern Recognition*, pages 4578–4587, 2021. [1](#), [2](#)
- [60] Zehao Yu, Songyou Peng, Michael Niemeyer, Torsten Sattler, and Andreas Geiger. Monosdf: Exploring monocular geometric cues for neural implicit surface reconstruction. *Advances in neural information processing systems*, 35:25018–25032, 2022. [1](#), [2](#)
- [61] Jiawei Zhang, Jiahe Li, Xiaohan Yu, Lei Huang, Lin Gu, Jin Zheng, and Xiao Bai. Cor-gs: sparse-view 3d gaussian splatting via co-regularization. In *European Conference on Computer Vision*, pages 335–352. Springer, 2024. [2](#)
- [62] K. Zhang, G. Riegler, N. Snavely, and V. Koltun. Nerf++: Analyzing and Improving Neural Radiance Fields. In *arXiv Preprint*, 2020. [1](#), [2](#)
- [63] Richard Zhang, Phillip Isola, Alexei A Efros, Eli Shechtman, and Oliver Wang. The Unreasonable Effectiveness of Deep Features as a Perceptual Metric. In *Conference on Computer Vision and Pattern Recognition*, pages 586–595, 2018. [7](#)
- [64] Jinghao Zhou, Chen Wei, Huiyu Wang, Wei Shen, Cihang Xie, Alan Yuille, and Tao Kong. ibot: Image bert pre-training with online tokenizer. *arXiv preprint arXiv:2111.07832*, 2021. [2](#)
- [65] Hanxin Zhu, Tianyu He, Xin Li, Bingchen Li, and Zhibo Chen. Is vanilla mlp in neural radiance field enough for few-shot view synthesis? In *Proceedings of the IEEE/CVF Conference on Computer Vision and Pattern Recognition*, pages 20288–20298, 2024. [2](#)